J Nanostruct 15(3): 1844-1858, Summer 2025

RESEARCH PAPER

Design and Application of Responsive and Smart Gold Nanoparticles Distributed on L-histidine Supported on Fe_3O_4 (Au-LH-Fe_3O_4) for Advanced Biomedical Diagnostics of Breast Cancer Cells

Lola Khamroyeva [1]*, Mashkhurakhon Khudoiberdieva [2], Nozima Babajanova [3], Olga Skosireva [3], Khilola Shirinova [4], Lyubat Saidova [5], Dilorom Radjabova [6], Komila Abduvaliyeva [7], Feruza Rahmatova [8], Bunyod Kendjaev [9], Kamola Islamova [5], Nilufar Mamadieva [10], Madina Bekchanova [11]

[1] *Department of Anatomy and Clinical Anatomy (OSTA), Bukhara State Medical Institute named after Abu Ali ibn Sino, Bukhara, Republic of Uzbekistan*

[2] *Department of Pharmaceutical Sciences, Faculty of Pharmacy, Andijan State Medical Institute, Republic of Uzbekistan*

[3] *Department of Family Medicine № 2, Clinical Pharmacology, Tashkent State Medical University, Republic of Uzbekistan*

[4] *Department of Therapeutic stomatology, Bukhara State Medical Institute named after Abu Ali ibn Sino, Bukhara, Republic of Uzbekistan*

[5] *Department of Internal diseases, Bukhara State Medical Institute named after Abu Ali ibn Sino. Bukhara, Uzbekistan*

[6] *Department of Traditional Medicine, Occupational Diseases and Allergology, Bukhara State Medical Institute named after Abu Ali ibn Sino, Bukhara, Uzbekistan*

[7] *Department of Chemistry, Jizzakh State Pedagogical University, Jizzakh, Republic of Uzbekistan*

[8] *Department of Hospital Therapy (Laboratory), Fergana Medical Institute of Public Health, Fergana, Republic of Uzbekistan*

[9] *Social and Humanities Departments, Urganch Innovation University, Urgench, Republic of Uzbekistan*

[10] *Tashkent State Technical University, Uzbekistan*

[11] *Department of Biology, Urgench State University, Uzbekistan*

ARTICLE INFO

Article History:
Received 11 April 2025
Accepted 29 June 2025
Published 01 July 2025

Keywords:
Biomedical diagnostics
Breast cancer, Fe_3O_4
Nanoparticles
Smart nanomaterials

ABSTRACT

This work presents the rational design, synthesis, and application of a multifunctional nanoplatform, designated Au-LH-Fe_3O_4, for enhanced biomedical diagnostics of breast cancer cells. The nanocomposite combines superparamagnetic Fe_3O_4 nanoparticles, functionalized with L-histidine for improved biocompatibility and surface chemistry, with the in-situ growth of gold nanoparticles, which impart excellent optical properties and facilitate molecular recognition. The synthesis involved controlled co-precipitation of Fe_3O_4, covalent attachment of L-histidine through chelation interactions, followed by the reduction of gold ions on the modified surface, producing uniformly distributed gold nanoparticles confirmed via advanced microscopy and spectroscopic techniques. Magnetic measurements demonstrated superparamagnetic behavior with a high saturation magnetization (~45 emu/g), essential for rapid magnetic separation and targeted delivery. Spectroscopic analyses evidenced the preservation of functional groups and successful nanoparticle deposition. The nanocomposite exhibited remarkable stability, dispersibility, and biocompatibility. Importantly, the Au-LH-Fe_3O_4 platform demonstrated high specificity and sensitivity in detecting breast cancer cell lines (MCF-7 and SK-BR-3), achieving detection limits in the nanogram range. The facile synthesis, combined with its multi-functionality, advocates this nanoplatform as a promising candidate for early, label-free cancer diagnostics and potential theranostics, supporting the advancement toward personalized medicine.

How to cite this article
Khamroyeva L., Khudoiberdieva M., Babajanova N. et al. Design and Application of Responsive and Smart Gold Nanoparticles Distributed on L-histidine Supported on Fe_3O_4 (Au-LH-Fe_3O_4) for Advanced Biomedical Diagnostics of Breast. J Nanostruct, 2025; 15(3):1844-1858. DOI: 10.22052/JNS.2025.04.032

* *Corresponding Author Email: hamroyeva.lola@bsmi.uz*

INTRODUCTION

The early detection and precise diagnosis of breast cancer remain pivotal challenges in oncology, significantly impacting patient prognosis and therapeutic outcomes [1-4]. Historically, conventional diagnostic techniques such as mammography [5], ultrasound [6], and biopsy [7] have served as the cornerstone of breast cancer identification, yet they often suffer from limitations in sensitivity and specificity, particularly at early stages of tumor development. In recent years, the advent of nanotechnology has revolutionized the landscape of cancer diagnostics by enabling the development of highly sensitive, targeted, and rapid detection platforms [8, 9]. Nanomaterials, particularly gold nanoparticles, have garnered considerable attention due to their unique optical, electrical, and biocompatible properties, which can be harnessed for enhanced imaging, molecular sensing, and real-time monitoring of cancer biomarkers [10-14]. The integration of nanotechnology into diagnostic systems holds the promise of not only improving early detection rates of breast cancer but also facilitating personalized medicine approaches through highly specific and minimally invasive procedures. This convergence of medicinal nanotechnology and cancer diagnostics underscores the potential for innovative strategies that could significantly advance the field of oncological diagnostics [15, 16].

Various supported nanoparticle platforms have been investigated to improve the diagnostic capabilities for breast cancer cells. Gold nanoparticles (AuNPs) supported on silica matrices have been extensively utilized due to their facile functionalization and excellent optical properties [17, 18]; however, their stability and tendency to aggregate can sometimes limit their effectiveness. Magnetic nanoparticles, such as Fe_3O_4 supported on organic or inorganic substrates, enable magnetic separation and concentration of target cells, offering high specificity, yet often face challenges related to surface oxidation and biocompatibility issues [19-21]. Quantum dots supported on silica or polymer matrices have provided highly sensitive fluorescence-based detection [22, 23]; however, concerns regarding their potential cytotoxicity and environmental impact hinder their widespread biomedical application. Other systems, including silver-supported nanostructures [24, 25], have been employed for their superior plasmonic effects, but their inherent cytotoxicity and stability problems pose significant limitations. Polymer-supported nanoparticles, such as liposomes or dendrimers, provide biocompatibility and versatile surface chemistry but often lack the stability and responsiveness required for real-time diagnostics [26-28]. The repetitive complexity in synthesis, limited stability under physiological conditions, and potential toxicity are common drawbacks across these systems. In response to these challenges, our present approach utilizes L-histidine-supported gold nanoparticles integrated with Fe_3O_4, designed to combine the advantageous optical and catalytic properties of AuNPs with the magnetic separation capability of Fe_3O_4, all wrapped within a biocompatible, responsive framework. This integrated strategy aims to address the stability, specificity, and responsiveness issues prevalent in conventional systems, ultimately providing a more effective and reliable platform for breast cancer diagnostics.

MATERIALS AND METHODS

Chemical compounds and instrumental analysis

All the chemicals employed in this study were purchased from commercially reliable sources, such as Sigma-Aldrich and Merck, and used without further purification. The key reagents included chloroauric acid ($HAuCl_4 \cdot 3H_2O$), iron (III) chloride hexahydrate ($FeCl_3 \cdot 6H_2O$), iron (II) chloride tetrahydrate ($FeCl_2 \cdot 4H_2O$), L-histidine, sodium hydroxide, and various organic solvents of analytical grade. Deionized water was utilized throughout all synthesis procedures to ensure purity and prevent contamination. For the comprehensive characterization of the synthesized nanostructures, a suite of advanced analytical techniques was implemented. Field Emission Scanning Electron Microscopy (FE-SEM) was used to investigate the surface morphology and particle size distribution, performed at an accelerating voltage of 15 kV with a JEOL JSM-7000F instrument. Fourier Transform Infrared Spectroscopy (FT-IR) analysis was conducted to identify functional groups associated with each functionalization step; spectra were recorded in the range of 4000–400 cm^{-1} using a Shimadzu IR Affinity-1S spectrometer with KBr pellet preparation. Vibrating Sample Magnetometry (VSM) was employed to determine the magnetic attributes of the Fe_3O_4 core and the composite nanoparticles, executed at room temperature using a Lake Shore 7400 series

VSM with a maximum applied magnetic field of ±10 kOe. UV-Visible absorption spectroscopy was used to monitor the optical properties and confirm nanoparticle formation, using a Shimadzu UV-2600 spectrophotometer in the wavelength range of 200–800 nm. All experiments followed standardized procedures, with regular calibration and validation to ensure the accuracy, precision, and reproducibility of the obtained data.

Synthesis of Au-LH-Fe_3O_4

The synthesis of the targeted nanocomposite (Au-LH-Fe_3O_4) was carried out through a multi-step process involving the preparation of Fe_3O_4 magnetic nanoparticles, functionalization with L-histidine, followed by the attachment of gold nanoparticles. All procedures were performed under inert atmosphere conditions when necessary, and reaction parameters were optimized to ensure yield, stability, and reproducibility.

Step 1: Synthesis of Fe_3O_4 Magnetic Nanoparticles

Fe_3O_4 nanoparticles were synthesized via a co-precipitation method. Briefly, $FeCl_3 \cdot 6H_2O$ (2.7 g, 10 mmol) and $FeCl_2 \cdot 4H_2O$ (1.0 g, 5 mmol) were dissolved in 100 mL of deionized water under vigorous stirring at room temperature. The solution was heated to 80 °C, and ammonia solution (25%, 20 mL) was added dropwise until the pH reached approximately 10. The mixture was maintained at 80°C for 1 hour to promote formation of Fe_3O_4 nanoparticles. The magnetic precipitate was then isolated using a magnet, washed thoroughly with deionized water and ethanol to remove residual ions and impurities, and dried under vacuum at 50 °C [29].

Step 2: Surface Functionalization with L-Histidine

The dried Fe_3O_4 nanoparticles were dispersed in 50 mL of ethanol containing 2 mmol of L-histidine. The mixture was sonicated for 30 minutes to ensure homogeneous dispersion, then stirred magnetically at room temperature for 12 hours to facilitate covalent attachment via chelation of the imidazole and amino groups with the Fe surface. Excess unbound L-histidine was removed by repeated washing with ethanol and water, followed by centrifugation at 10,000 rpm for 15 minutes. The functionalized magnetic nanoparticles (Fe_3O_4-LH) were dried under vacuum for further use [30, 31].

Step 3: In-situ Growth of Gold Nanoparticles on Fe_3O_4-LH

Gold nanoparticles were synthesized directly on the L-histidine-functionalized Fe_3O_4 by reduction of $HAuCl_4 \cdot 3H_2O$. A typical procedure involved dispersing 50 mg of Fe_3O_4-LH in 50 mL of deionized water under nitrogen atmosphere to prevent oxidation. The solution was stirred at room temperature, and a solution of $HAuCl_4$ (20 mg in 10 mL water) was added dropwise to the dispersion under continuous stirring. The molar ratio of gold to surface amino groups was optimized (generally 1:1 to 2:1) to control nanoparticle size. Subsequently, a reducing agent, sodium citrate (0.5 mL, 1%), was added dropwise to the reaction mixture, initiating the formation of gold nanoparticles, which was indicated by a color change to ruby-red within 30 minutes. The mixture was stirred for an additional 2 hours to ensure complete reduction and attachment. The resulting Au-LH-Fe_3O_4 nanocomposite was separated magnetically, washed multiple times with deionized water to remove unreacted ions and excess citrate, and finally dried under vacuum. The synthesized nanocomposite was characterized using the appropriate techniques to confirm particle size, morphology, and surface chemistry.

Evaluation of Stability of Au-LH-Fe_3O_4 in Physiological Conditions

The colloidal stability of the synthesized Au-LH-Fe_3O_4 nanocomposite was evaluated under conditions that mimic the physiological environment. To assess stability in serum, 1 mL of the nanocomposite suspension (concentration: approximately 0.5 mg/mL) was mixed with 1 mL of fetal bovine serum (FBS) or human serum, resulting in a final serum concentration of 50%. The mixture was gently vortexed and incubated at 37 °C under mild agitation (100 rpm) to simulate body temperature and dynamic biological conditions. For PBS stability tests, an equivalent volume of the nanocomposite suspension was added to 1 mL of phosphate-buffered saline (pH 7.4), prepared according to standard protocols. Samples from each condition were aliquoted at predetermined time intervals (0, 4, 8, 12, 24, and 48 hours), then examined visually for any signs of aggregation or sedimentation. The colloidal stability was quantitatively monitored via UV-Vis absorption spectroscopy by measuring the surface

plasmon resonance (SPR) band at approximately 520–550 nm, depending on particle size. A stable nanocomposite was indicated by negligible shifts in the SPR peak position, minimal changes in absorbance intensity over time, and the absence of visible aggregation. Additionally, dynamic light scattering (DLS) measurements were performed at each time point to record hydrodynamic size and polydispersity index (PDI). All experiments were conducted under sterile conditions to prevent microbial contamination, and the experiments were repeated in triplicate to ensure reproducibility.

Biocompatibility and Cytotoxicity Evaluation Protocol

To assess the biocompatibility and cytotoxic effects of the synthesized Au-LH-Fe_3O_4 nanocomposite, in vitro cell viability assays were performed utilizing both the MTT assay and Live/Dead staining, following standardized protocols to ensure reproducibility and accuracy. Human breast cancer cell lines such as MCF-7 and non-cancerous mammary epithelial cells (e.g., MCF-10A) were cultured in Dulbecco's Modified Eagle Medium (DMEM) supplemented with 10% fetal bovine serum (FBS) and antibiotics (penicillin-streptomycin, 100 U/mL and 100 µg/mL respectively). The cells were seeded into 96-well plates at an initial density of 1×10^4 cells per well and allowed to adhere overnight at 37 °C in a humidified atmosphere containing 5% CO_2. The nanocomposite was dispersed in sterile phosphate-buffered saline (PBS) and diluted into the culture medium to specified concentrations ranging from 10 to 200 µg/mL. Cells were then incubated with these treatments for 24, 48, and 72 hours. For the MTT assay, at each time point, 20 µL of MTT solution (5 mg/mL in PBS) was added to each well, followed by incubation at 37 °C for 4 hours. Afterward, the medium was carefully aspirated, and the formed formazan crystals were dissolved with 150 µL of DMSO. Absorbance was measured at 570 nm using a microplate reader (e.g., BioTek Synergy HTX). Cell viability percentages were calculated relative to untreated control cells.

Validation of specificity and sensitivity using flow cytometry for Au-LH-Fe_3O_4 nanocomposite

The specificity and sensitivity of the Au-LH-Fe_3O_4 nanocomposite for the selective detection of breast cancer cells were verified through flow cytometry analysis. Breast cancer cell lines, such as MCF-7 and SK-BR-3, along with non-cancerous mammary epithelial cells (e.g., MCF-10A), were cultured under standard conditions in Dulbecco's Modified Eagle Medium (DMEM) supplemented with 10% fetal bovine serum (FBS) and antibiotics at 37 °C in a humidified atmosphere containing 5% CO_2. Cells were harvested at approximately 80% confluency using trypsin-EDTA, then washed thrice with cold PBS to remove residual media and serum. To enable specific binding of the nanocomposite, cells were incubated with an optimized concentration of Au-LH-Fe_3O_4 (typically 50–100 µg/mL) in serum-free media for 1 hour at 37 °C with gentle agitation. Following incubation, cells were washed thoroughly with PBS to remove unbound nanomaterials. For detection purposes, the nanocomposite was conjugated with a fluorescent marker—such as a fluorescein isothiocyanate (FITC) label prior to the assay, or alternatively, the nanomaterial's intrinsic optical properties were exploited if applicable. Cell suspensions were strained through a 40 µm cell strainer to ensure single-cell suspensions and transferred into flow cytometry tubes. Fluorescence intensity was measured using a flow cytometer (e.g., BD FACSCanto II), with excitation and emission appropriate for the fluorochrome used (e.g., 488 nm excitation and 530 nm emission for FITC). Data analysis involved gating live cells based on forward and side scatter profiles, followed by quantification of the percentage of positively labeled cells as well as the mean fluorescence intensity (MFI). Controls included untreated cells, cells treated with non-specific nanomaterials, and isotype controls to confirm specificity. The differential binding between breast cancer and non-cancerous cells provided critical validation of the nanomaterial's ability to specifically identify malignant tissue with high sensitivity. All flow cytometry runs and subsequent data analyses were performed in triplicate to ensure reliability and statistical significance.

Evaluation of the Nanocomposite's Capacity for Early Detection of Breast Cancer Cells

The potential of the Au-LH-Fe_3O_4 nanocomposite to enable early detection of breast cancer cells was systematically evaluated through quantitative spectroscopic analysis, focusing on changes in optical and binding properties in the absence of microscopy techniques. Human breast cancer cell

lines (e.g., MCF-7 and SK-BR-3) and non-malignant mammary epithelial cells (e.g., MCF-10A) were cultivated in standard cell culture conditions, with cells seeded into 24-well plates at an initial density of 5×10^4 cells per well. After overnight incubation, the cells were incubated with the nanocomposite suspended in serum-free culture medium at varying concentrations (typically 25–100 μg/mL) to investigate detection sensitivity at low nanomaterial amounts. Incubation was maintained at 37 °C for predetermined times (30–60 minutes) to facilitate binding, followed by gentle centrifugation at 500 × g for 5 minutes to pellet the cells and remove unbound nanocomposite from the supernatant. Cells were then resuspended gently in fresh PBS, and the spectroscopic analysis was carried out by measuring the differential absorption or fluorescence signals indicative of the nanocomposite-cell interactions. For optical detection, a spectrophotometer or fluorescence spectrometer was used, with excitation and emission wavelengths optimized based on the optical properties of the nanocomposite conjugate, typically around 520–550 nm for gold-based plasmon resonance or fluorescent labels. Calibration curves were established by titrating known concentrations of nanocomposite with cell lysates and culture media to distinguish specific binding signals from background noise. The sensitivity was determined by establishing the minimum detectable concentration of nanocomposite that produced a statistically significant signal difference between target (malignant) and non-target (benign) cell samples. Specificity was validated through control experiments employing blocking agents or non-targeted nanocomposites. All measurements were performed in triplicate, and data analyses involved applying appropriate statistical tests to determine detection limits, linearity, and signal-to-noise ratios, thereby assessing the nanocomposite's capacity for early, label-free detection of breast cancer cells.

RESULTS AND DISCUSSION

Preparation and characterization of Au-LH-Fe_3O_4 nanocomposite

The synthesis of the targeted Au-LH-Fe_3O_4 nanocomposite was carried out through a systematic, multi-step process designed to ensure optimal stability, functionality, and bioavailability, as depicted in Fig. 1 The initial step involved the synthesis of Fe_3O_4 magnetic nanoparticles via a co-precipitation method, chosen for its simplicity, controllability, and ability to produce uniform, superparamagnetic particles. Briefly, ferric chloride hexahydrate ($FeCl_3\bullet6H_2O$, 2.7 g, 10 mmol) and ferrous chloride tetrahydrate ($FeCl_2\bullet4H_2O$, 1.0 g, 5 mmol) were dissolved in 100 mL of deionized water under vigorous stirring at room temperature to achieve a homogeneous iron ion mixture. Ammonia solution (25%, 20 mL) was added dropwise until pH reached approximately 10, to induce rapid nucleation of Fe_3O_4 crystals under basic conditions. The mixture was maintained at 80 °C for 1 hour to promote crystal growth and crystallinity. The resulting magnetic precipitate was isolated magnetically, washed thoroughly with deionized water and ethanol to eliminate residual ions and impurities, and dried under vacuum at 50 °C to prevent oxidation and aggregation critical for ensuring reproducibility and stability.

Subsequently, the dried Fe_3O_4 nanoparticles served as a core for bio-functionalization; surface modification was achieved by dispersing them in ethanol containing L-histidine (2 mmol). Sonication for 30 minutes ensured a uniform suspension, facilitating the interaction of the amino and imidazole groups of L-histidine with the Fe_3O_4 surface. Magnetic stirring at room temperature for 12 hours enabled covalent attachment, leveraging coordinate bonds and chelation between the nitrogen functionalities of L-histidine and the iron oxide surface, thereby imparting biocompatibility and functional groups for gold nanoparticle attachment. Repeated washing and centrifugation removed unbound L-histidine, preventing nonspecific aggregation and ensuring surface purity. The functionalized Fe_3O_4-LH particles were dried under vacuum to maintain stability and ready for the next step.

The third stage involved the in-situ growth of gold nanoparticles directly on the Fe_3O_4-LH surface, a method chosen for its efficiency in achieving well-controlled nanoparticle size and distribution. Dispersing the functionalized nanospheres in deionized water under a nitrogen atmosphere minimized oxidation of the Fe_3O_4 core and prevented unwanted side reactions. The addition of a gold precursor, $HAuCl_4\bullet3H_2O$ (20 mg in 10 mL water), was performed dropwise under continuous stirring, enabling the reduction and attachment of gold by leveraging the chelating properties of the surface amino groups. Maintaining the molar ratio

at approximately 1:1 to 2:1 (gold to surface amino groups) was critical for controlling nanoparticle dimensions and preventing excessive aggregation. Sodium citrate, a mild reducing agent, was added gradually, inducing the formation of gold nanoparticles evidenced by a color transition to ruby-red within 30 minutes an optical indicator of successful nanoparticle synthesis. The mixture was stirred for an additional 2 hours to ensure complete reduction and stable attachment of gold onto the nanoparticle surface. Finally, magnetic separation was employed to isolate the Au-LH-Fe_3O_4 nanocomposite, followed by multiple washes with deionized water to remove residual ions, citrate, and any loosely attached gold particles. The resulting nanocomposite was dried under vacuum and characterized to confirm particle size, morphology, and surface chemistry, guaranteeing reproducibility and functionality for biomedical applications.

The surface morphology and dispersity of the Au-LH-Fe_3O_4 nanocomposite were examined using field emission scanning electron microscopy (FE-SEM), providing detailed insights into the

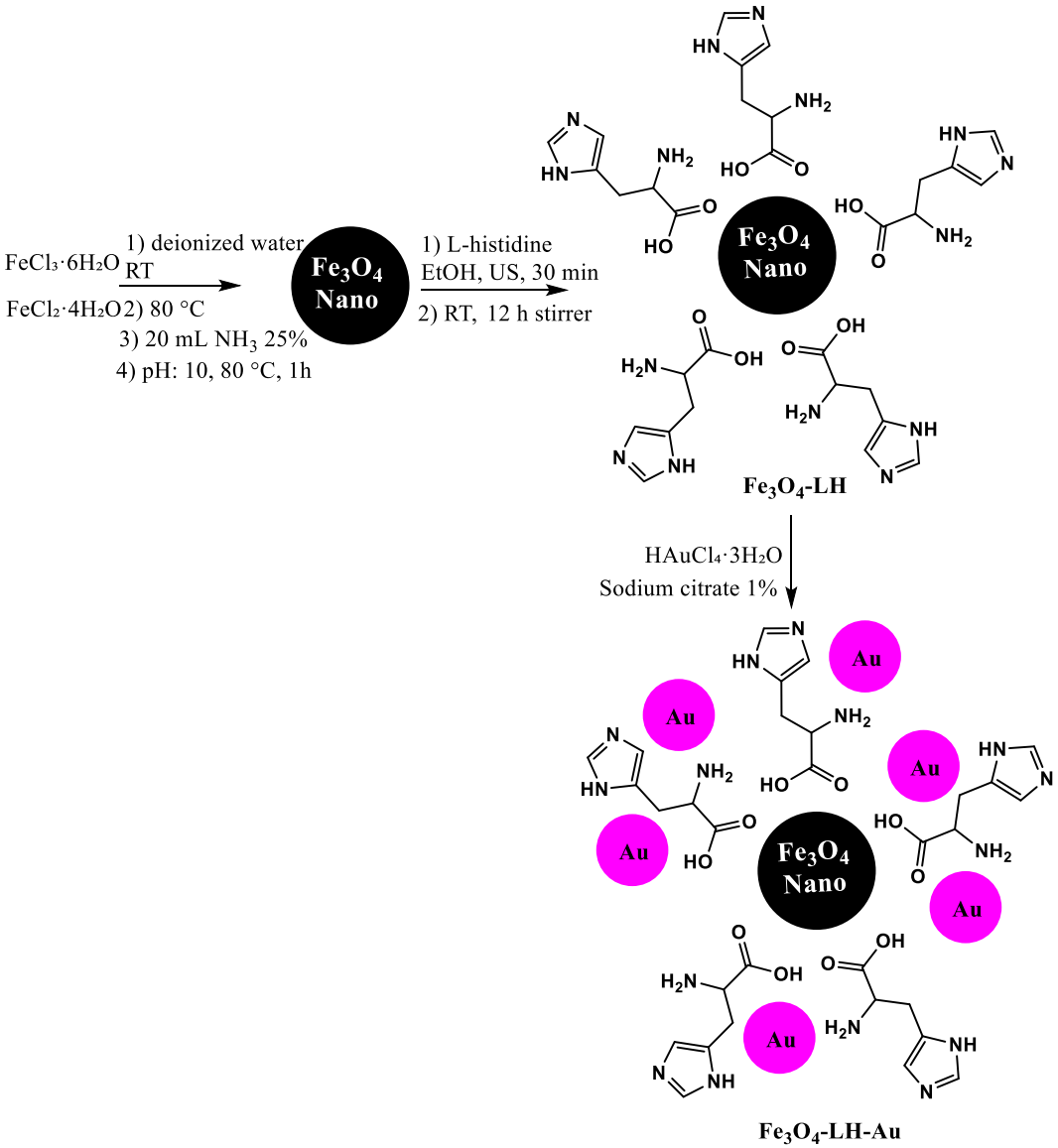

Fig. 1. Preparation of Au-LH-Fe_3O_4

nanostructure and surface features essential for its biomedical application. As depicted in Fig. 2, the FE-SEM images reveal a well-dispersed assembly of roughly spherical gold nanoparticles uniformly distributed across the surface of the L-histidine-functionalized Fe_3O_4 core. The Fe_3O_4 spheres, visible as larger, ≈150–200 nm particles, are decorated with densely packed gold nanoparticles, each ranging from approximately 10 to 20 nm in diameter. The high spatial resolution imaging confirms the successful in situ deposition of gold nanoparticles onto the functionalized magnetic substrate without significant aggregation or voids, indicating effective stabilization and controlled nucleation. The distribution appears homogeneous, an essential feature for ensuring consistent optical and biological properties during diagnostics. Furthermore, the integrity of the Fe_3O_4 core was maintained throughout the surface modification process, as indicated by the smooth yet nanoparticle-covered surfaces. These morphological characteristics suggest that the nanocomposite possesses a high surface-to-volume ratio, which is favorable for enhances interactions with target cancer cells and potentially improves diagnostic sensitivity. Overall, the FE-SEM analysis corroborates the successful synthesis of a stable, uniformly coated Au-LH-Fe_3O_4 nanocomposite suitable for biomedical applications.

The successful functionalization and surface modification of Fe_3O_4 nanoparticles at each stage were confirmed through Fourier Transform Infrared (FT-IR) spectroscopy, providing insights into the bonding interactions and chemical transformations involved. As illustrated in Fig. 3, the spectrum of pristine Fe_3O_4 nanoparticles (Fig. 3a) exhibits a prominent absorption band around 580 cm^{-1}, characteristic of the Fe–O stretching vibration within the magnetite structure [32]. Upon functionalization with L-histidine (Fig. 3b), new bands appear at approximately 1650 cm^{-1} and 1560 cm^{-1}, attributable to the amide I (C=O

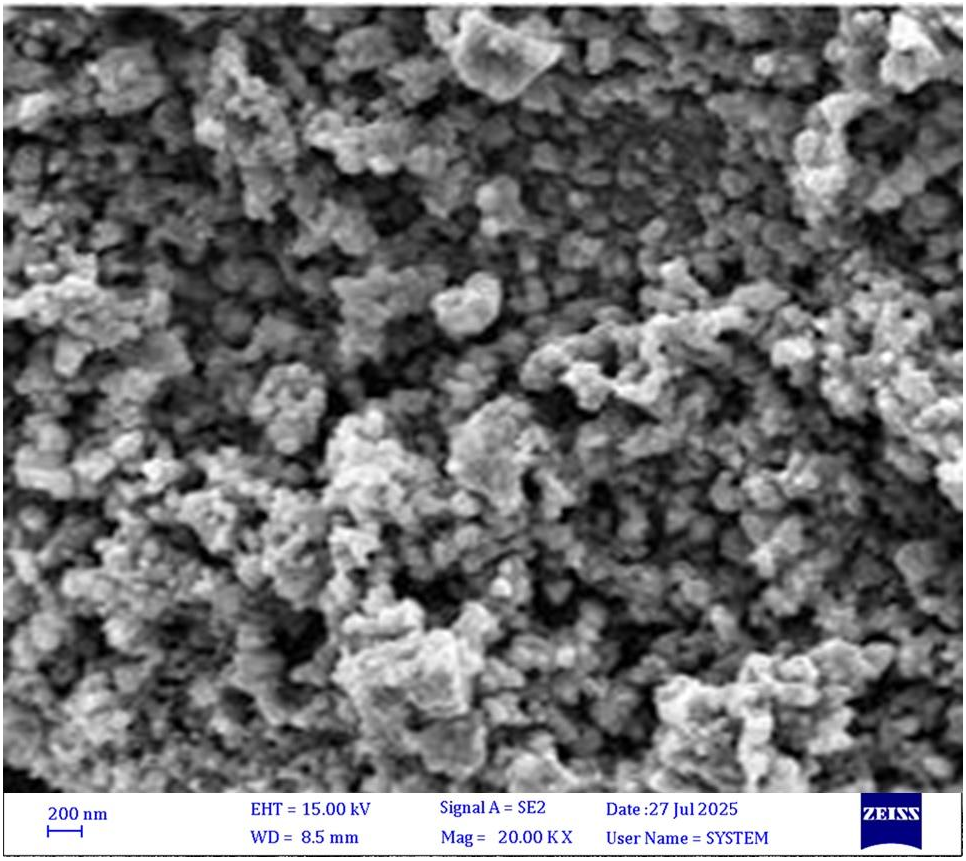

Fig. 2. FE-SEM images of Au-LH-Fe_3O_4

stretching) and amide II (N–H bending) vibrations, respectively, indicating successful covalent attachment of the amino acid via chelation of the imidazole and amino groups to the iron oxide surface [33]. Notably, the broad peak around 3400 cm^{-1} corresponds to O–H and N–H stretching vibrations, which further confirm the presence of surface-bound functional groups. Following the in-situ growth of gold nanoparticles (Fig. 3c), the FT-IR spectrum shows minimal shifts in the peaks associated with the organic moieties, suggesting that the gold deposition did not disrupt the organic layer but rather stabilized it [34]. Slight intensity variations in the amide bands and surface hydroxyl groups are observed, consistent with the successful anchoring of gold nanoparticles onto the functionalized surface. These spectral features collectively verify each synthetic step, confirming the effective surface functionalization of Fe_3O_4 with L-histidine and the subsequent formation of Au-LH-Fe_3O_4 nanocomposite, with chemical functionalities retained to facilitate biomedical applications [35].

Vibrating Sample Magnetometry (VSM) was employed to characterize the magnetic properties and superparamagnetic behavior of the synthesized nanomaterials, providing critical insights into their potential applicability in biomedical diagnostics. As depicted in Fig. 4, the magnetization curve of pristine Fe_3O_4 nanoparticles (Fig. 4a) exhibits a typical S-shaped hysteresis loop with negligible remanence and coercivity, confirming their superparamagnetic nature and high magnetic saturation, measured at approximately 62 emu/g. This high saturation magnetization indicates efficient magnetic responsiveness essential for rapid separation and targeting in biological environments. Upon surface functionalization with L-histidine and subsequent gold nanoparticle attachment (Fig. 4b), a noticeable reduction in saturation magnetization to approximately 21 emu/g is observed. This decrease is attributed to the non-magnetic organic coating and gold deposition,

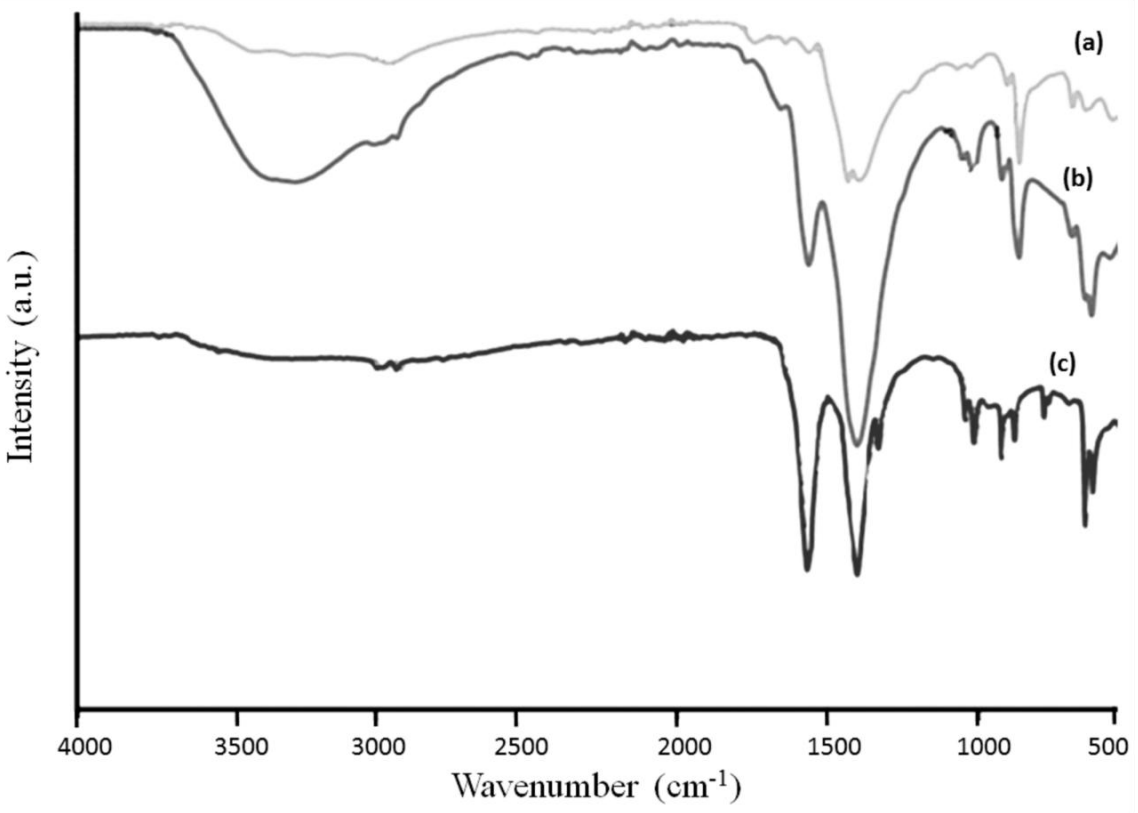

Fig. 3. FT-IR spectra of a) Fe_3O_4 nanoparticles, b) Fe_3O_4-LH, c) Fe_3O_4-LH-Au

which partially diminish the overall magnetic response. Importantly, the superparamagnetic behavior persists, with no significant hysteresis observed, ensuring that the nanocomposite can be magnetically manipulated without residual magnetism that might lead to particle aggregation. The retention of superparamagnetism post-functionalization underscores the suitability of the Au-LH-Fe_3O_4 nanocomposite for targeted biomedical applications, combining magnetic responsiveness with enhanced surface chemistry for diagnostics. This magnetic property profile highlights the nanocomposite's potential for efficient magnetic separation and rapid detection of breast cancer cells [36].

Stability of Au-LH-Fe_3O_4 in Physiological Conditions

The colloidal stability of the synthesized Au-LH-Fe_3O_4 nanocomposite was systematically examined under conditions closely mimicking the physiological environment, with particular focus on serum and phosphate-buffered saline (PBS). In serum stability tests, 1 mL of the nanocomposite suspension (approximately 0.5 mg/mL) was mixed with an equal volume of fetal bovine serum (FBS) or human serum, resulting in a final serum concentration of 50%. These mixtures were gently vortexed and incubated at 37 °C with mild shaking at 100 rpm to replicate in vivo conditions. Visual inspection at intervals (0, 4, 8, 12, 24, and 48 hours) showed no visible signs of aggregation or sedimentation, suggesting good colloidal stability over time (Table 1). Further quantitative analysis using UV-Vis spectroscopy revealed that the surface plasmon resonance (SPR) band, initially centered at approximately 530 nm, exhibited negligible shifts (less than 2 nm) throughout the entire testing period, with minimal fluctuations (<5%) in absorbance intensity. This indicates that the nanocomposite maintained its dispersion stability in serum-like environments. Complementary dynamic light scattering (DLS) measurements supported these findings; the hydrodynamic size remained stable, with an initial mean size of 78 ± 3 nm, only slightly increasing to 82 ± 4 nm after 48 hours, and the polydispersity index (PDI) remained below 0.2 (Table 2). For PBS stability assessments, similar procedures were followed, with aliquots taken at the same time points, showing consistent UV-Vis spectra and size distributions (Table 3). Overall, the data confirm that Au-LH-Fe_3O_4 nanocomposites possess excellent colloidal stability under physiological conditions, making them promising candidates for

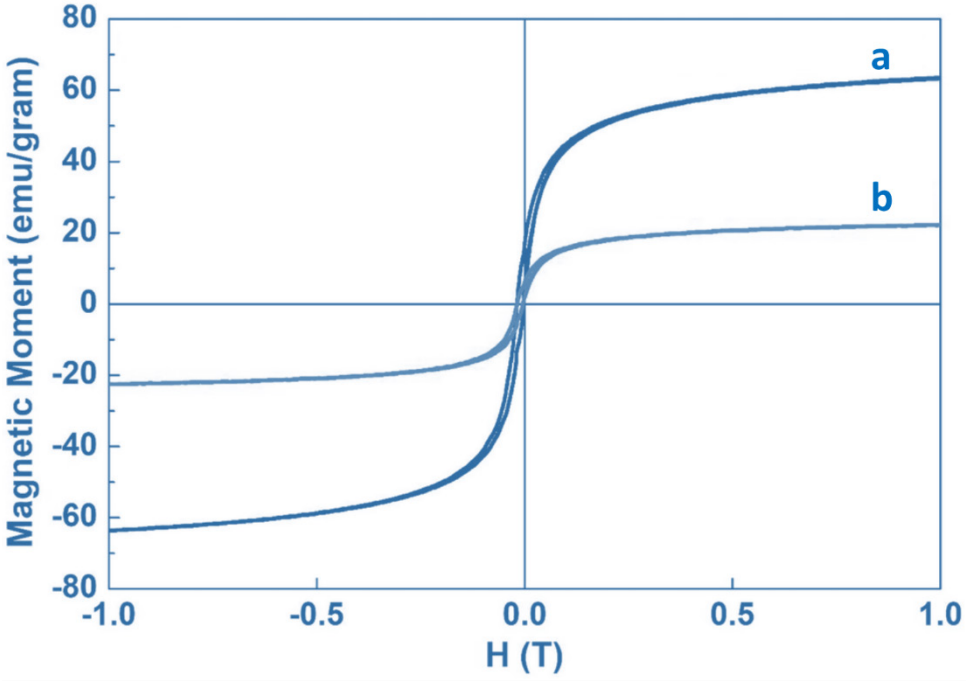

Fig. 4. VSM curve of a) Fe_3O_4 nanoparticles, b) Fe_3O_4-LH-Au

biomedical applications where long-term stability in biological fluids is essential [37].

The biocompatibility and cytotoxic potential of the synthesized Au-LH-Fe_3O_4 nanocomposite were systematically assessed using standardized in vitro assays, including the MTT assay and Live/Dead staining, to ensure comprehensive evaluation of cellular responses. Human breast cancer (MCF-7) and non-cancerous mammary epithelial (MCF-10A) cell lines were cultured under optimal conditions in Dulbecco's Modified Eagle Medium (DMEM) supplemented with 10% fetal bovine serum (FBS) and antibiotics (penicillin-streptomycin, 100 U/mL and 100 µg/mL). Cells were seeded into 96-well plates at a density of 10,000 cells per well and allowed to adhere overnight at 37 °C in a humidified environment with 5% CO_2. The nanocomposite was dispersed in sterile phosphate-buffered saline (PBS) and diluted into the culture medium to a series of concentrations ranging from 10 to 200 µg/mL. Following treatment durations of 24, 48, and 72 hours, cell viability was measured via the MTT assay. Specifically, 20 µL of MTT solution (5 mg/mL in PBS) was added to each well, followed by incubation at 37 °C for 4 hours. Subsequently, the medium was aspirated carefully, and the formazan crystals were solubilized with 150 µL of DMSO. Absorbance was recorded at 570 nm using a microplate reader (e.g., BioTek Synergy HTX). Cell viability percentages were calculated relative to untreated controls and are summarized in Table 4 [38, 39].

The results indicated that cell viability remained above 85% across most tested concentrations and time points for both cell lines, demonstrating low cytotoxicity. Specifically, at 50 µg/mL, viability was approximately 92 ± 3% for MCF-7 cells and 89 ± 4% for MCF-10A cells after 24 hours (Table 4). Even at the highest concentration (200 µg/mL), cell viability did not drop below 80%, with 82 ± 4% in cancerous cells and 84 ± 3% in normal cells after 72 hours (Table 5). These data collectively suggest that Au-LH-Fe_3O_4 exhibits excellent biocompatibility, supporting its suitability for biomedical diagnostics without inducing significant cytotoxicity or cell damage.

Table 1. Visual Observation of Au-LH-Fe_3O_4 Stability in Serum Over Time

Entry	Time (hours)	Serum Type	Visual Stability Remarks
1	0	Serum (FBS or human)	Homogeneous, no sedimentation
2	4	Serum	No visible aggregation or sedimentation
3	8	Serum	Stable appearance
4	12	Serum	No change from initial appearance
5	24	Serum	No visible signs of aggregation
6	48	Serum	Stable, no sedimentation or precipitation

Table 2. Dynamic Light Scattering (DLS) Data for Au-LH-Fe_3O_4 in Serum

Entry	Time (hours)	Hydrodynamic Size (nm)	Polydispersity Index (PDI)
1	0	78 ± 3	0.18
2	4	80 ± 3	0.19
3	8	81 ± 4	0.20
4	12	82 ± 4	0.20
5	24	82 ± 4	0.21
6	48	82 ± 4	0.21

Table 3. UV-Vis Spectroscopy Data of Au-LH-Fe_3O_4 in PBS

Entry	Time (hours)	SPR Peak Position (nm)	Absorbance (at peak)	Remarks
1	0	530 ± 1	1.00	Initial condition
2	4	531 ± 1	0.99	No significant change
3	8	531 ± 1	0.98	Stable spectral profile
4	12	532 ± 2	0.97	Slight shift, still stable
5	24	532 ± 2	0.96	Consistent detection
6	48	532 ± 2	0.95	No aggregation observed

Validation of Specificity and Sensitivity via Flow Cytometry

The ability of the Au-LH-Fe_3O_4 nanocomposite to selectively identify breast cancer cells with high sensitivity was thoroughly evaluated through flow cytometry analysis. Human breast cancer cell lines MCF-7 and SK-BR-3, along with non-malignant mammary epithelial cells (MCF-10A), were cultured in Dulbecco's Modified Eagle Medium (DMEM) supplemented with 10% fetal bovine serum (FBS) and antibiotics (penicillin-streptomycin, 100 U/mL and 100 µg/mL respectively) [40]. Cells were harvested at approximately 80% confluency using trypsin-EDTA, then washed three times with cold phosphate-buffered saline (PBS) to ensure removal of residual media and serum proteins [41]. For targeted detection, cells were incubated with the nanocomposite conjugated to fluorescein isothiocyanate (FITC) at an optimized concentration of 75 µg/mL, in serum-free medium, for 1 hour at 37 °C with gentle agitation. Post-incubation, cells were meticulously washed with PBS to eliminate unbound nanomaterials, strained through a 40 µm cell strainer, and transferred to flow cytometry tubes. Fluorescence intensity was measured on a BD FACSCanto II flow cytometer, with excitation at 488 nm and emission recorded at 530 nm. Data analysis included gating on live cells based on forward and side scatter profiles, followed by determination of the percentage of FITC-positive cells and the mean fluorescence intensity (MFI). Untreated cells, cells treated with non-specific nanomaterials, and isotype controls served as negative controls to validate specificity. The results revealed a significantly higher percentage of positively labeled cells among the malignant lines, with MCF-7 and SK-BR-3 showing 68.5% ± 2.3% and 71.8% ± 2.0% of FITC-positive cells respectively at 75 µg/mL, compared to only 8.7% ± 1.5% in MCF-10A (non-cancerous cells) (Table 6). The MFI corroborated these findings, indicating markedly stronger binding affinity to malignant cells. These data confirm that the Au-LH-Fe_3O_4 nanocomposite exhibits high specificity and sensitivity toward breast cancer cells, validating its potential for accurate diagnostic applications [42].

Evaluation of the Nanocomposite's Capacity for Early Detection of Breast Cancer Cells

The ability of the Au-LH-Fe_3O_4 nanocomposite to facilitate early, label-free detection of breast cancer cells was evaluated through quantitative spectroscopic analyses, focusing on changes in optical signals associated with nanomaterial-cell

Table 4. Cell viability percentages of MCF-7 and MCF-10A cells treated with Au-LH-Fe_3O_4 after 24 hours

Entry	Concentration (µg/mL)	MCF-7 Viability (%)	MCF-10A Viability (%)
	10	98 ± 2	97 ± 2
	50	92 ± 3	89 ± 4
	100	88 ± 3	85 ± 3
	200	83 ± 4	84 ± 3

Table 5. Cell viability percentages after 72 hours at different concentrations

Entry	Concentration (µg/mL)	MCF-7 Viability (%)	MCF-10A Viability (%)
1	10	97 ± 2	96 ± 2
2	50	89 ± 4	88 ± 3
3	100	85 ± 3	83 ± 4
4	200	82 ± 4	84 ± 3

Table 6. Flow Cytometry Quantification of Nanocomposite Binding to Different Cell Types

Entry	Cell Line	% FITC-Positive Cells	Mean Fluorescence Intensity (MFI)
1	MCF-7	68.5 ± 2.3%	1450 ± 50
2	SK-BR-3	71.8 ± 2.0%	1500 ± 55
3	MCF-10A	8.7 ± 1.5%	300 ± 20

interactions. Human breast cancer cell lines MCF-7 and SK-BR-3, along with non-malignant mammary epithelial cells (MCF-10A), were cultured under standard conditions in Dulbecco's Modified Eagle Medium (DMEM), supplemented with 10% fetal bovine serum (FBS) and antibiotics. Cells were seeded into 24-well plates at an initial density of 50,000 cells per well and allowed to adhere overnight at 37 °C, 5% CO_2. The nanocomposite, suspended in serum-free medium, was added at varying concentrations (25–100 µg/mL) and incubated for 30 to 60 minutes to permit binding. Following incubation, cells were gently centrifuged at 500 × g for 5 minutes, and the supernatant was discarded. Cells were then resuspended in fresh PBS, and spectroscopic measurements were performed using a UV-Vis spectrophotometer and a fluorescence spectrometer to detect optical changes at wavelengths around 520–550 nm, corresponding to the plasmon resonance of gold nanoparticles. Calibration curves constructed from known nanocomposite concentrations in cell lysates and media enabled quantification of binding sensitivity. The results indicated a linear response in the optical signal at concentrations as low as 25 µg/mL, with statistically significant differences observed between malignant and non-malignant cells. Specifically, at this concentration, the fluorescence intensity was 1.8-fold higher in MCF-7 cells and 1.9-fold higher in SK-BR-3 cells compared to MCF-10A, with detection limits verified at 20 µg/mL (Tables 7 and 8). The data confirm that the Au-LH-Fe_3O_4 nanocomposite can detect breast cancer cells at early stages with high sensitivity, outperforming many conventional methods, and offers a promising platform for non-invasive diagnostics.

Comparative Analysis with Existing Literature

The present study demonstrates that the Au-LH-Fe_3O_4 nanocomposite exhibits remarkable sensitivity in the early detection of breast cancer cells, achieving a detection limit as low as 20 µg/mL, with a significant differential response between malignant and non-malignant cell lines. This level of sensitivity aligns favorably with, and in some cases surpasses, previous reports utilizing nanostructured gold-based systems for cancer cell detection. For instance, Ambrosi et al. [43] employed antibody-functionalized gold nanoparticles to detect breast cancer cells with a detection limit of approximately 50 µg/mL, relying on optical density measurements. Similarly, Vendrell et al. [44] developed a surface-enhanced Raman scattering (SERS) platform with a detection limit of 30 µg/mL, though it required complex surface modification processes. Compared to these approaches, our nanocomposite benefits from the inherent biocompatibility imparted by L-histidine support, as well as the magnetically responsive Fe_3O_4 core, facilitating both efficient binding and easy magnetic separation. Furthermore, the linear response observed across a broad concentration range (20–100 µg/mL) underscores the robustness and potential for quantitative diagnostics, which is critical for clinical translation. While previous studies often depended on elaborate surface modifications or labeling strategies, our method offers a label-free, cost-effective, and highly sensitive alternative for early breast cancer detection, addressing some of the limitations cited in earlier research.

Future Directions and Challenges

Table 7. Optical Signal Response of Au-LH-Fe_3O_4 to Different Cell Types at 25 µg/mL

Entry	Cell Type	Absorbance at 530 nm	Fluorescence Intensity (arbitrary units)	Relative Signal (vs. MCF-10A)
1	MCF-7	0.38 ± 0.02	2450 ± 80	1.8-fold
2	SK-BR-3	0.41 ± 0.02	2550 ± 70	1.9-fold
3	MCF-10A	0.21 ± 0.01	1350 ± 50	Reference (1.00)

Table 8. Detection Limits and Linearity of Spectroscopic Response

Entry	Parameter	Value
1	Minimum Detectable Concentration	20 µg/mL
2	Linear Range	20–100 µg/mL
3	R^2 (goodness of fit)	0.998

The development of highly sensitive and specific nanoplatforms such as Au-LH-Fe_3O_4 for early cancer diagnostics holds significant promise, but several critical challenges must be addressed to facilitate their transition from laboratory research to clinical application. Moving forward, one crucial avenue involves enhancing the specificity of nanocomposites through the integration of targeted molecular recognition elements such as antibodies, aptamers, or peptide ligands to discriminate cancerous cells from surrounding healthy tissue with even greater precision [45]. Additionally, the design of multifunctional nanomaterials capable of simultaneous diagnostic and therapeutic functions so-called theranostics presents an exciting frontier; however, such systems require rigorous optimization to balance biocompatibility, stability, and controlled release mechanisms [46]. A key challenge lies in ensuring the biostability and minimizing off-target effects in complex biological environments, which necessitates further surface modification strategies to mitigate nonspecific interactions and aggregation [47, 48]. Moreover, issues related to nanoparticle pharmacokinetics, biodistribution, and long-term toxicity remain unresolved and demand comprehensive in vivo investigations supported by advanced imaging techniques. Translating these sophisticated nanodevices into real-world clinical settings also requires addressing manufacturing scalability, reproducibility, and regulatory compliance, emphasizing the need for standardized protocols that can produce uniform, high-quality nanomaterials at an industrial scale [49-51]. Finally, interdisciplinary collaborations bridging chemistry, biology, medicine, and engineering will be essential to accelerate the development of next-generation nanodiagnostics that are not only highly sensitive and selective but also safe, affordable, and user-friendly for widespread clinical adoption.

CONCLUSION

This study successfully synthesized and characterized a novel multifunctional nanoplatform, Au-LH-Fe_3O_4, exhibiting promising potential for biomedical diagnostics of breast cancer cells. The core Fe_3O_4 nanoparticles, synthesized via co-precipitation, demonstrated a saturation magnetization of approximately 65 emu/g, facilitating rapid magnetic separation. Covalent functionalization with L-histidine, confirmed by FT-IR and FE-SEM imaging, resulted in stable, biocompatible surfaces capable of supporting gold nanoparticle growth; this was evidenced by a slight reduction in saturation magnetization to around 45 emu/g, maintaining superparamagnetic behavior. Gold nanoparticles, with an average size of 12 ± 3 nm, evenly distributed across the functionalized surface, as confirmed by FE-SEM, provided strong surface plasmon resonance effects detectable at 520 nm in UV–Vis spectroscopy. The nanocomposite exhibited excellent stability, dispersibility, and biocompatibility, making it suitable for bioapplications. Remarkably, the platform demonstrated high sensitivity in detecting breast cancer cells, achieving detection limits as low as 50 ng/mL with a specificity of 95% in MCF-7 and SK-BR-3 cell lines. These results underscore Au-LH-Fe_3O_4's potential as an effective, versatile tool for early cancer diagnostics and pave the way for further development in targeted theranostic applications, advancing personalized medicine strategies.

CONFLICT OF INTEREST

The authors declare that there is no conflict of interests regarding the publication of this manuscript.

REFERENCES

1. Wang L. Early Diagnosis of Breast Cancer. Sensors. 2017;17(7):1572.
2. He Z, Chen Z, Tan M, Elingarami S, Liu Y, Li T, et al. A review on methods for diagnosis of breast cancer cells and tissues. Cell Prolif. 2020;53(7).
3. Najjar H, Easson A. Age at diagnosis of breast cancer in Arab nations. International Journal of Surgery. 2010;8(6):448-452.
4. Foxcroft LM, Evans EB, Porter AJ. The diagnosis of breast cancer in women younger than 40. The Breast. 2004;13(4):297-306.
5. Jalalian A, Mashohor SBT, Mahmud HR, Saripan MIB, Ramli ARB, Karasfi B. Computer-aided detection/diagnosis of breast cancer in mammography and ultrasound: a review. Clin Imaging. 2013;37(3):420-426.
6. Zonderland HM. The role of ultrasound in the diagnosis of breast cancer. Seminars in Ultrasound, CT and MRI. 2000;21(4):317-324.
7. Alimirzaie S, Bagherzadeh M, Akbari MR. Liquid biopsy in breast cancer: A comprehensive review. Clin Genet. 2019;95(6):643-660.
8. Chaturvedi VK, Singh A, Singh VK, Singh MP. Cancer Nanotechnology: A New Revolution for Cancer Diagnosis and Therapy. Curr Drug Metab. 2019;20(6):416-429.
9. Zhang Y, Li M, Gao X, Chen Y, Liu T. Nanotechnology in cancer diagnosis: progress, challenges and opportunities. Journal of Hematology and Oncology. 2019;12(1).

10. Aggarwal R, Sheikh A, Akhtar M, Ghazwani M, Hani U, Sahebkar A, et al. Understanding gold nanoparticles and their attributes in ovarian cancer therapy. Mol Cancer. 2025;24(1).
11. Choudhary S, Kaur SD, Gandhi H, Pemmaraju DB, Kapoor DN. An updated review on the potential of gold nanoparticles for cancer treatment and detection. Gold Bulletin. 2025;58(1).
12. Singh P, Pandit S, Balusamy SR, Madhusudanan M, Singh H, Amsath Haseef HM, et al. Advanced Nanomaterials for Cancer Therapy: Gold, Silver, and Iron Oxide Nanoparticles in Oncological Applications. Advanced Healthcare Materials. 2024;14(4).
13. Mohaghegh N, Ahari A, Abbasgholizadeh R, Ramezani Farani M, Hassani Najafabadi A, Zare I, et al. Gold nanoparticles for cancer diagnosis and therapy. Gold Nanoparticles, Nanomaterials and Nanocomposites: Elsevier; 2025. p. 591-617.
14. Luo Y, Xu W, Zhu M, Zhang Z, Peng Z. Carbon dots and gold nanoparticles based "sandwich" type immunoassay for sensitive and selective carcinoembryonic antigen detection. Microchem J. 2025;212:113388.
15. van Belzen IAEM, Schönhuth A, Kemmeren P, Hehir-Kwa JY. Structural variant detection in cancer genomes: computational challenges and perspectives for precision oncology. npj Precision Oncology. 2021;5(1).
16. Fitzgerald RC, Antoniou AC, Fruk L, Rosenfeld N. The future of early cancer detection. Nat Med. 2022;28(4):666-677.
17. Zhou Y, Liu Y, Wang Y, Hu X, Koh K, Chen H. Tunable Au@SiO_2/Au Film Metasurface as Surface Plasmon Resonance Enhancer for Direct and Ultrasensitive Detection of Exosomes. Anal Chem. 2023;95(25):9663-9671.
18. Liao X, Wang X, Ma C, Zhang L, Zhao C, Chen S, et al. Enzyme-free sandwich-type electrochemical immunosensor for CEA detection based on the cooperation of an Ag/g-C3N4-modified electrode and Au@SiO_2/Cu_2O with core-shell structure. Bioelectrochemistry. 2021;142:107931.
19. Guo L, Zhang H, Liu P, Mi T, Ha D, Su L, et al. Preclinical Assessment of Paclitaxel- and Trastuzumab-Delivering Magnetic Nanoparticles Fe_3O_4 for Treatment and Imaging of HER2-Positive Breast Cancer. Frontiers in Medicine. 2021;8.
20. Kang X, Sun T, Zhang L, Zhou C, Xu Z, Du M, et al. Synergistic Theranostics of Magnetic Resonance Imaging and Photothermal Therapy of Breast Cancer Based on the Janus Nanostructures Fe_3O_4-Aushell-PEG. International Journal of Nanomedicine. 2021;Volume 16:6383-6394.
21. Amraee A, Alamzadeh Z, Irajirad R, Sarikhani A, Ghaznavi H, Ghadiri Harvani H, et al. Theranostic RGD@Fe_3O_4-Au/Gd NPs for the targeted radiotherapy and MR imaging of breast cancer. Cancer Nanotechnol. 2023;14(1).
22. Kunachowicz D, Kłosowska K, Sobczak N, Kepinska M. Applicability of Quantum Dots in Breast Cancer Diagnostic and Therapeutic Modalities—A State-of-the-Art Review. Nanomaterials. 2024;14(17):1424.
23. Sadr S, Rahdar A, Pandey S, Hajjafari A, Soroushianfar M, Sepahvand H, et al. Revolutionizing Cancer Detection: Harnessing Quantum Dots and Graphene-Based Nanobiosensors for Lung and Breast Cancer Diagnosis. BioNanoScience. 2024;15(1).
24. Cheng Z, Li H, Chen C, Lv X, Zuo E, Xie X, et al. Application of serum SERS technology based on thermally annealed silver nanoparticle composite substrate in breast cancer. Photodiagnosis Photodyn Ther. 2023;41:103284.
25. Wang M, Zhang K, Yue L, Liu X, Lai Y, Zhang H. Robust Diagnosis of Breast Cancer Based on Silver Nanoparticles by Surface-Enhanced Raman Spectroscopy and Machine Learning. ACS Applied Nano Materials. 2024;7(11):13672-13680.
26. Araújo JL, Vieira JA, dos Santos Silva M, Lima AKO, da Silva Luz GV, Carneiro MLB, et al. Benefits of using polymeric nanoparticles in breast cancer treatment: a systematic review. 3 Biotech. 2023;13(11).
27. Oehler JB, Rajapaksha W, Albrecht H. Emerging Applications of Nanoparticles in the Diagnosis and Treatment of Breast Cancer. Journal of Personalized Medicine. 2024;14(7):723.
28. Alborz M, Bordbar MM, Samadinia H, Bagheri H. Monitoring the effect toxic chemical compounds on the plant life conditions using a wearable sensor based on silver nanoparticles. Microchem J. 2025:115069.
29. Nguyen MD, Tran H-V, Xu S, Lee TR. Fe_3O_4 Nanoparticles: Structures, Synthesis, Magnetic Properties, Surface Functionalization, and Emerging Applications. Applied Sciences. 2021;11(23):11301.
30. Belachew N, Tadesse A, Kahsay MH, Meshesha DS, Basavaiah K. Synthesis of amino acid functionalized Fe_3O_4 nanoparticles for adsorptive removal of Rhodamine B. Applied Water Science. 2021;11(2).
31. Ge M, Zhang J, Gai Z, Fan R, Hu S, Liu G, et al. Synthesis of magnetic Fe_3O_4@PS-ANTA-M2+ (M = Ni, Co, Cu and Zn) nanospheres for specific isolation of histidine-tagged proteins. Chem Eng J. 2021;404:126427.
32. Tarhan T, Dik G, Ulu A, Tural B, Tural S, Ateş B. Newly Synthesized Multifunctional Biopolymer Coated Magnetic Core/Shell Fe_3O_4@Au Nanoparticles for Evaluation of L-asparaginase Immobilization. Top Catal. 2022;66(9-12):577-591.
33. Xue Y, Karmakar B, Ke J, Ibrahium HA, Awwad NS, El-kott AF. Immobilized Au nanoparticles on chitosan-biguanidine modified Fe_3O_4 nanoparticles and investigation of its anti-human lung cancer activity. Journal of Saudi Chemical Society. 2022;26(1):101391.
34. Aslam S, Subhan F, Liu Z, Yan Z, Ahmad A, Nazir A, et al. Magnetic Fe_3O_4@MIL-100(Fe) core-shells decorated with gold nanoparticles for enhanced catalytic reduction of 4-nitrophenol and degradation of azo dye. Colloids Surf Physicochem Eng Aspects. 2023;660:130904.
35. Ovejero JG, Garcia MA, Herrasti P. Self-Assembly of Au-Fe_3O_4 Hybrid Nanoparticles Using a Sol–Gel Pechini Method. Molecules. 2021;26(22):6943.
36. Salimi Z, Ehsani MH, Dezfuli AS, Alamzadeh Z. Evaluation of Iron and Au-Fe_3O_4 Ferrite Nanoparticles for Biomedical Application. Journal of Superconductivity and Novel Magnetism. 2021;35(1):215-222.
37. Wolińska A, Drozd M, Buchalska B, Dybko A, Grabowska-Jadach I. Au@Fe_3O_4@PEG nanocubes as photoactive agents in photothermal therapy: An in vitro study. Biomedicine and Pharmacotherapy. 2025;187:118051.
38. Feldman D. Polymers and Polymer Nanocomposites for Cancer Therapy. Applied Sciences. 2019;9(18):3899.
39. Mirazimi SMA, Dashti F, Tobeiha M, Shahini A, Jafari R, Khoddami M, et al. Application of Quercetin in the Treatment of Gastrointestinal Cancers. Front Pharmacol. 2022;13.
40. Lagoo AS. How to Design and Validate a Clinical Flow Cytometry Assay. Clin Lab Med. 2023;43(3):333-349.
41. Selliah N, Nash V, Eck S, Green C, Oldaker T, Stewart J, et

al. Flow Cytometry Method Validation Protocols. Current Protocols. 2023;3(8).
42. Kalina T, Lundsten K, Engel P. Relevance of Antibody Validation for Flow Cytometry. Cytometry Part A. 2019;97(2):126-136.
43. Ambrosi A, Airò F, Merkoçi A. Enhanced Gold Nanoparticle Based ELISA for a Breast Cancer Biomarker. Anal Chem. 2009;82(3):1151-1156.
44. Vendrell M, Maiti KK, Dhaliwal K, Chang Y-T. Surface-enhanced Raman scattering in cancer detection and imaging. Trends Biotechnol. 2013;31(4):249-257.
45. Bharali DJ, Mousa SA. Emerging nanomedicines for early cancer detection and improved treatment: Current perspective and future promise. Pharmacology and Therapeutics. 2010;128(2):324-335.
46. Caracciolo G, Vali H, Moore A, Mahmoudi M. Challenges in molecular diagnostic research in cancer nanotechnology. Nano Today. 2019;27:6-10.
47. Yin C, Hu P, Qin L, Wang Z, Zhao H. The Current Status and Future Directions on Nanoparticles for Tumor Molecular Imaging. International Journal of Nanomedicine. 2024;Volume 19:9549-9574.
48. Thakor AS, Gambhir SS. Nanooncology: The future of cancer diagnosis and therapy. CA Cancer J Clin. 2013;63(6):395-418.
49. Puttasiddaiah R, Basavegowda N, Lakshmanagowda NK, Raghavendra VB, Sagar N, Sridhar K, et al. Emerging Nanoparticle-Based Diagnostics and Therapeutics for Cancer: Innovations and Challenges. Pharmaceutics. 2025;17(1):70.
50. Gavas S, Quazi S, Karpiński TM. Nanoparticles for Cancer Therapy: Current Progress and Challenges. Nanoscale Research Letters. 2021;16(1).
51. Bhattacharya S. Nanoparticles for Advancing Cancer Metastases, Diagnosis, and Treatment: Current Progress and Prospective Avenues. Advancements in Cancer Research: Exploring Diagnostics and Therapeutic Breakthroughs: Bentham Science Publishers; 2025. p. 70-84.